Fluid ratcheting by oscillating channel walls with sawteeth

Jie Yu[1,2,†]

[1]Civil Engineering Program, Department of Mechanical Engineering, Stony Brook University, Stony Brook, NY 11794, USA

[2]School of Marine and Atmospheric Sciences, Stony Brook University, Stony Brook, NY 11794, USA

A laboratory experiment shows that fluid can be pumped from one end to another in a narrow channel whose sawtooth walls vibrate transversely opposite to each other. The phenomenon is referred to as ratcheting fluid. Inspired by this, we put forward here a theory describing the rectified steady flow, and the net directional pumping. In a conformally transformed plane, the induced steady streaming in the Stokes boundary layer of the oscillatory flow is analysed, elucidating the driving mechanism that is due to the nonlinearity and viscosity. The solution of the stream function is given, showing the complex spatial structure of the induced steady flow and its spatial average that is related to the directional pumping. Whereas the wall sawtooth shape is the primary source of asymmetry, the difference in entrance and exit flow conditions due to the geometries at channel ends is found to be a secondary source to break the left–right symmetry of the system. This latter can affect the net directional transport of fluid, in particular in short channels with a small number of sawteeth. Various influences on the net pumping rate are analysed.

---

1. Introduction

Motions rectified by symmetry-breaking mechanisms in oscillating flows have been of great interest in biological locomotion and engineering applications (e.g. van Oeveren & Houghton 1971; Mahadevan, Daniel & Chaudhury 2003; Spagnolie & Shelley 2009). Thiria & Zhang (2010) demonstrated experimentally that in a narrow channel between two parallel plates, with their facing sides lined with asymmetrical sawteeth, fluid can be pumped from one end to the other in the channel when the plates oscillate transversely against each other; see figure 1. Those are one-dimensional periodical arrays of sawteeth. Since the directional transport is achieved without valves, this demonstration of ratcheting fluid using geometric asymmetry also offers an alternative idea for valveless pumps, which remain active interests in applications of microfluidics and biomedical engineering (Auerbach, Moehring & Moser 2004; Rinderknecht, Hickerson & Gharib 2005).

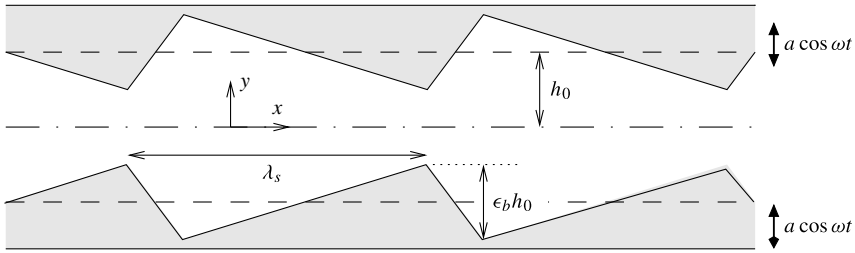† Email address for correspondence: Jie.Yu.1@stonybrook.edu

FIGURE 1. A two-dimensional model of the channel with oscillating walls, showing the geometry and relevant scales.

In oscillating flows, the importance of viscosity in inducing a steady streaming has long been known, since Rayleigh (1883) studied circulations induced by standing oscillations in air. For propagating water waves, steady streaming in Stokes boundary layers was first fully determined by Longuet-Higgins (1953), who also clarified Eulerian and Lagrangian streaming. The latter is also known as mass transport. Owing to nonlinear convective inertia, the time periodic fluctuations lead to a time-averaged momentum flux (analogous to Reynolds stresses) which drives a secondary steady flow against viscous resistance (Mei 1989). Of course, the rectification of time oscillations does not necessarily provide a unidirectional transport of fluid, unless the spatial symmetry is broken. In the case of standing waves, the oscillation intensity varies between nodes and antinodes of the surface envelope, resulting in a spatially periodic variation of the steady momentum flux. However, because of the left–right symmetry in standing waves, the induced steady flow in the Stokes boundary layer consists of a pair of closed circulating cells between two adjacent nodes (or antinodes). This steady circulation flow field has zero spatial average, producing no net transport of fluid mass in either direction. In contrast, the induced steady flow in the boundary layer under a traveling wave is unidirectional because the time oscillation is associated with a spatial 'bias' set by the wave propagation. This unidirectional flow causes mass to drift in the direction of wave near the boundary. This action of mass transport is what Longuet-Higgins (1983) referred to as the peristaltic pumping in water waves. The mechanism is in fact shared by peristaltic transport occurring in many physiological and biological applications.

For pure oscillatory motions over a non-flat boundary, e.g. a rippled seabed, the oscillation intensity near the boundary is rendered to be non-uniform in space, leading to a spatially varying steady momentum flux. As a result, steady circulations can be induced in the Stokes layer. If the boundary structure is spatially symmetric, these steady circulations would have zero spatial average, hence having no ability to transport fluid unidirectionally. This is known from previous studies of symmetrical sand ripples (e.g. Hara & Mei 1990; Mei & Yu 1997). With a ratchet-like (or sawtooth) boundary structure, the spatial symmetry is broken, and the induced secondary steady flow is expected to have a non-zero spatial average leading to a pumping action. The ratcheting effect in Thiria & Zhang's experiment is akin to this. Motivated by the experiment, we here propose a theory to describe the ratcheting effects of fluids in a narrow channel with its sawtooth walls subject to harmonic oscillations normal to the channel centreline. To deal with large sawteeth, we shall adapt the conformal transformation method that has recently been developed for wave propagation over periodic topographies (Yu & Howard 2012). Whereas the method of

constructing the map applies to profiles of arbitrary shape and magnitude, we shall in this study restrict our attention to cases where the sawteeth have large peak-to-trough height but long wavelength relative to the mean channel width. Thus, we can invoke a boundary-layer approximation which is 'terrain-following'. The analytical solution obtained elucidates the essential physics and clarifies various effects influencing the net pumping.

The rest of the paper is organized as follows. In §2, we present the equations describing the problem and the conformal transformation. In §3, an approximate theory is formulated, and the solutions are given for the rectified steady flow field and the net directional pumping rate. Some mathematical details are referred to appendices. Discussions are made in §4, examining various effects on the net flow rate. Concluding remarks follow in §5.

2. Mathematical description of the problem

Consider the motion of an incompressible fluid in a narrow channel between two parallel strips of rigid plates whose facing sides are each lined with a periodic array of sawteeth. The plates oscillate normal to the channel centreline and oppositely to each other, driving fluid motions; see sketch in figure 1. Suppose the sawtooth profile is one-dimensional, and described as $y' = \pm y'_s(x')$, where $y' = 0$ is the centreline of the channel. The primes denote dimensional variables. For time-harmonic oscillations of amplitude a and angular frequency ω, the movements of the plates are written as $y' = \pm y'_s(x') \pm a \cos \omega t'$. The amplitude a should be set such that the opposite sawteeth do not collide. In view of the symmetry with respect to the centreline, we shall consider just one half of the flow domain, say $y' \geqslant 0$.

Let $\boldsymbol{u}' = u'\boldsymbol{i} + v'\boldsymbol{j}$ be the velocity vector, whence

$$(u', v') = \left(\frac{\partial \psi'}{\partial y'}, -\frac{\partial \psi'}{\partial x'} \right), \tag{2.1}$$

where $\psi'(x', y', t')$ is the stream function. The vorticity $\boldsymbol{\nabla}' \times \boldsymbol{u}' = -\nabla^2 \psi' \boldsymbol{k}$ is a pseudo-vector perpendicular to the (x', y') plane. We shall scale the problem to be π-periodic by defining a wavenumber $k = \pi/\lambda_s$, where λ_s is the sawtooth wavelength, and choose the following normalization:

$$x = kx', \quad y = ky', \quad t = t'\omega, \quad \psi = \psi'/(a\omega/k). \tag{2.2a-d}$$

This implies $(u, v) = (u', v')(a\omega)^{-1}$. The dimensionless equation for the vorticity is

$$\frac{\partial}{\partial t} \nabla^2 \psi - \alpha\beta \frac{\partial \left(\psi, \nabla^2 \psi \right)}{\partial (x, y)} = \frac{1}{2}\sigma^2\beta^2 \nabla^2 \nabla^2 \psi, \quad 0 < y < y_s(x) + \alpha\beta \cos t, \tag{2.3}$$

where the nonlinear convection terms are written using the notation of Jacobian determinant $\partial(\psi, \nabla^2\psi)/\partial(x, y)$. The parameters are defined as

$$\alpha = a/h_0, \quad \beta = kh_0, \quad \sigma = \delta/h_0, \tag{2.4a-c}$$

where $\delta = \sqrt{2\nu/\omega}$ is the Stokes boundary-layer thickness, ν is the kinematic viscosity, and h_0 is the mean half channel width in the absence of motion. At the centreline,

$$\psi = 0, \quad \frac{\partial^2 \psi}{\partial y^2} = 0, \quad \text{at } y = 0. \tag{2.5a,b}$$

At the channel wall,

$$\frac{\partial \psi}{\partial y} = 0, \quad \frac{\partial \psi}{\partial x} = \sin t, \quad \text{at } y = y_s(x) + \alpha\beta \cos t. \tag{2.6a,b}$$

2.1. *The conformal transformation*

For periodic corrugations of arbitrary shape and amplitude, a conformal transformation can be constructed to map the flow domain onto a uniform strip (Yu & Howard 2012). This is adapted here. Let the undisturbed channel wall position be written as $y_s = kh_0 \left[1 + \epsilon_b f(x)\right]$, where $f(x)$ is the sawtooth profile, ϵ_b is a dimensionless amplitude parameter. We shall require $f(x)$ to have zero average in x, so that h_0 is the mean half channel width in the absence of motion. When $f(x)$ is so normalized that the peak-to-trough height is unity, $\epsilon_b h_0$ is the sawtooth height. We consider $\epsilon_b = O(1)$. Following Yu & Howard (2012), the mapping between the physical plane (x, y) and the mapped plane (ξ, η), is given by the transformation functions

$$x = \xi + \epsilon_b kh \sum_{j=1}^{\infty} \left(b_j \sin 2j\xi - c_j \cos 2j\xi\right) \cosh 2j\eta / \sinh 2jkh, \qquad (2.7)$$

$$y = \eta + \epsilon_b kh \sum_{j=1}^{\infty} \left(b_j \cos 2j\xi + c_j \sin 2j\xi\right) \sinh 2j\eta / \sinh 2jkh, \qquad (2.8)$$

where kh, and the coefficients b_j and c_j are determined by the channel wall profile. The Cauchy–Riemann conditions, $\partial x/\partial \xi = \partial y/\partial \eta$ and $\partial x/\partial \eta = -\partial y/\partial \xi$, can be readily verified. The centreline $y = 0$ is mapped into $\eta = 0$. The periodicity of the problem is preserved, as the map is periodic in x and in ξ with the same period π. By requiring $y = y_s(x)$ to be mapped into a straight line $\eta = kh$, we get

$$kh_0 + \epsilon_b kh_0 f(x) = kh + \epsilon_b kh \sum_{j=1}^{\infty} \left(b_j \cos 2j\xi + c_j \sin 2j\xi\right) \qquad (2.9)$$

with

$$x = \xi + \epsilon_b kh \sum_{j=1}^{\infty} \left(b_j \sin 2j\xi - c_j \cos 2j\xi\right) \coth (2jkh). \qquad (2.10)$$

Averaging (2.9) over a spatial period, recalling that $f(x)$ has zero average in x and using (2.10) to relate dx and dξ, we obtain

$$kh_0 = kh + (\epsilon_b kh)^2 \sum_{j=1}^{\infty} \left(b_j^2 + c_j^2\right) j \coth 2jkh. \qquad (2.11)$$

Solving (2.9)–(2.11), we determine kh, b_j and c_j for the given profile $f(x)$. Since y is antisymmetric and x is symmetric in η, the opposite channel wall at $y = -y_s$ is mapped into $\eta = -kh$. Under the transformation, the centreline remains to be a straight line at $\eta = 0$, while the corrugated channel walls are stretched to become flat surfaces at $\eta = \pm kh$. It is thus clear that kh is the dimensionless half channel width in the mapped plane, in the absence of wall movement. With the vibrations, the instantaneous wall position $y(x, t) = y_s(x) + \alpha\beta \cos t$ is mapped into a curve $\eta = \eta_{sw}(\xi, t)$, i.e. given $\left[x, y(x, t)\right]$, the inverse of the map (2.7) and (2.8) gives $[\xi, \eta_{sw}(\xi, t)]$. For relatively small amplitude of oscillations, this curve should be fairly close to $\eta = kh$.

The vorticity equation (2.3) is transformed into

$$\frac{\partial}{\partial t}\nabla^2\psi - \alpha\beta \frac{\partial \left(\psi, J^{-1}\nabla^2\psi\right)}{\partial \left(\xi, \eta\right)} = \frac{1}{2}\sigma^2\beta^2\nabla^2 \left(J^{-1}\nabla^2\psi\right), \quad 0 < \eta < \eta_{sw}(\xi, t), \qquad (2.12)$$

where

$$\nabla^2 = \frac{\partial^2}{\partial \xi^2} + \frac{\partial^2}{\partial \eta^2}, \qquad (2.13)$$

and the Jacobian of transformation is

$$J = \left(\frac{\partial x}{\partial \xi} \right)^2 + \left(\frac{\partial x}{\partial \eta} \right)^2. \tag{2.14}$$

Since

$$\frac{\partial \psi}{\partial \eta} = \frac{\partial \psi}{\partial x} \frac{\partial x}{\partial \eta} + \frac{\partial \psi}{\partial y} \frac{\partial y}{\partial \eta}, \quad \frac{\partial \psi}{\partial \xi} = \frac{\partial \psi}{\partial x} \frac{\partial x}{\partial \xi} + \frac{\partial \psi}{\partial y} \frac{\partial y}{\partial \xi}, \tag{2.15a,b}$$

the boundary conditions at the channel wall are written from (2.6) as

$$\frac{\partial \psi}{\partial \xi} = \frac{\partial x}{\partial \xi} \sin t, \quad \frac{\partial \psi}{\partial \eta} = \frac{\partial x}{\partial \eta} \sin t, \quad \text{at } \eta = \eta_{sw}(\xi, t). \tag{2.16a,b}$$

From (2.6), the boundary conditions at the centreline $\eta = 0$ are

$$\psi = 0, \quad \frac{\partial^2 \psi}{\partial \eta^2} = 0, \quad \text{at } \eta = 0. \tag{2.17a,b}$$

2.2. *The sawtooth wall profile*

An iterative algorithm for calculating the map is given in Yu & Howard (2012) which can determine the coefficients b_j and c_j, and kh with fairly good accuracy and efficiency, even for non-smooth functions such as square wave and sawtooth profiles. In this study, we shall smooth the 'conventional' sawtooth profile, avoiding the sharp corners and jumps thus removing the discontinuity from the function and its derivatives. This is to avoid the complications in the perturbation analysis, as follows, rather than any concerns on the computation of the map. The procedure of obtaining a smooth sawtooth profile that is exact to a prescribed map is as follows.

In one period $-\pi/2 \leqslant x \leqslant \pi/2$, an antisymmetric function for the 'conventional' sawtooth profile is written as

$$f_1(x) = \begin{cases} -(x + \pi/2)/(\pi - q) & \text{for } -\pi/2 \leqslant x \leqslant -q/2, \\ x/q & \text{for } -q/2 \leqslant x \leqslant q/2, \\ -(x - \pi/2)/(\pi - q) & \text{for } q/2 \leqslant x \leqslant \pi/2, \end{cases} \tag{2.18}$$

where q controls the skewness of the sawtooth. When $q = \pi/2$, $f_1(x)$ gives a symmetric sawtooth profile. When $q = 0$, $f_1(x)$ becomes discontinuous at $x = 0$, having a jump of magnitude 1. The Fourier series is

$$f_1(x) = \sum_{n=1}^{\infty} \frac{\sin nq}{n^2(\pi - q)q} \sin 2nx. \tag{2.19}$$

Using the first few terms of (2.19), we get a preliminary smooth profile $\widetilde{f}_1(x)$ for which we shall construct the conformal map satisfying (2.9)–(2.11). If we wish to use $\widetilde{f}_1(x)$ as the actual wall profile, we would have to keep as many terms of b_j and c_j as necessary, depending on the accuracy specified. We can also turn the problem around: we truncate the map just constructed to the first few terms, treating it as the new map and subsequently determining the shape of wall corrugations under this new map, i.e. explicitly calculating $[x(\xi, kh), f(x)]$. In this way, we obtain a sawtooth profile $f(x)$ for which we have an exact map that is expressed in a closed form with finite terms. The channel width kh_0 in the physical plane, that corresponds to the chosen
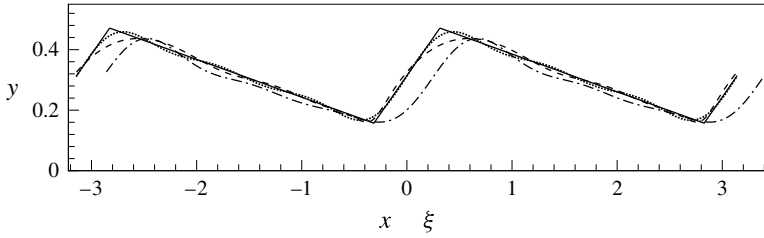
FIGURE 2. Sawtooth profiles at $y_s = kh_0 \left[1 + \epsilon_b f(x)\right]$: ——, conventional sawtooth $f(x) = f_1(x)$ given by (2.18) with $q = 0.2\pi$, $\epsilon_b = 1.0$, $kh_0 = 0.3142$ $(\lambda_s = 10h_0)$; $\cdots\cdots$, smooth profile $f(x) = \widetilde{f_1}(x)$ given by the first five terms of (2.19), for which b_j and c_j are computed; $---$, $f(x)$ given by the map which consists of the first three terms of b_j and c_j, $\epsilon_b = 1.0$, $kh_0 = 0.3130$; $-\cdot-$, $f(x)$ plotted in terms of ξ.

map and newly determined profile, is then evaluated from (2.11) using the appropriate terms. An example is shown in figure 2, comparing the sawtooth profiles at different stages of approximation. The parameter measuring the skewness $q = 0.2\pi$, meaning that the section of steep slope is approximately 20 % of the wavelength. The smooth sawtooth profile, given by the map consisting of the first three terms of b_j and c_j, is fairly similar to the conventional sawtooth geometry given by (2.18), except for its broadened troughs. In this example, the mean half channel width is $kh_0 = 0.3130$; with $\epsilon_b = 1.0$, the narrowest channel width at a sawtooth peak is approximately $y = 0.17$ from the centreline, and the maximum width at a sawtooth trough is approximately $y = 0.44$.

3. An approximation for narrow channels and weak oscillations

The large sawtooth amplitude necessitates the assumption of small oscillation amplitude to avoid collisions of sawtooth peaks. We shall focus on the cases in which $O(\alpha) = O(\beta) \ll 1$ and σ is finite, i.e. we consider the channel width h_0 to be narrow compared with sawtooth wavelength, the oscillation amplitude to be small compared with h_0 and the frequency to be moderate such that $\delta \sim h_0$. Since the sawtooth amplitude is comparable to h_0, the dominant slope of sawtooth is subsequently of $O(\beta)$. We also note that $\sigma^2 = 2\alpha/Re$, where $Re = a\omega h_0/\nu$ is the Reynolds number based on the width h_0 and velocity $a\omega$. The assumptions above imply that $Re = O(\alpha)$ or smaller for the overall channel flow.

In view of the aspect ratio, we introduce the rescaling $\widetilde{\eta} = \eta/\beta$, and rewrite from (2.12), (2.16) and (2.17)

$$\frac{\partial}{\partial t}\widetilde{\nabla}^2\psi - \alpha\frac{\partial(\psi, J^{-1}\widetilde{\nabla}^2\psi)}{\partial(\xi, \widetilde{\eta})} = \frac{1}{2}\sigma^2\widetilde{\nabla}^2(J^{-1}\widetilde{\nabla}^2\psi), \tag{3.1}$$

$$\frac{\partial\psi}{\partial\xi} = \frac{\partial x}{\partial\xi}\sin t, \quad \frac{\partial\psi}{\partial\widetilde{\eta}} = \beta\frac{\partial x}{\partial\eta}\sin t, \quad \text{at } \widetilde{\eta} = \beta^{-1}\eta_{sw}(\xi, t), \tag{3.2a,b}$$

$$\psi = 0, \quad \frac{\partial^2\psi}{\partial\widetilde{\eta}^2} = 0, \quad \text{at } \widetilde{\eta} = 0, \tag{3.3a,b}$$

where

$$\widetilde{\nabla}^2 = \frac{\partial^2}{\partial\widetilde{\eta}^2} + \beta^2\frac{\partial^2}{\partial\xi^2}. \tag{3.4}$$

The transformation functions are known and not rescaled, e.g. $\partial x / \partial \eta$ in (3.2a) is unchanged. The undisturbed wall is at $\widetilde{\eta} = \gamma$, where $\gamma \equiv h/h_0$. For $\beta \ll 1$, it follows from (2.14) that $J(\xi, \eta) = J_0(\xi) + O(\beta^2)$, where

$$J_0(\xi) = F^2, \quad F \equiv 1 + \epsilon_b \sum_{j=1}^{\infty} \left(b_j \cos 2j\xi + c_j \sin 2j\xi \right). \tag{3.5}$$

For $\alpha \ll 1$, the instantaneous wall position $\eta = \eta_{sw}(\xi, t)$ can be regarded as a perturbation from the undisturbed position $\eta = kh$. Let us identify the points forming the corrugated surface by their undisturbed positions (ξ_s, kh). Their positions at time t are $[\xi(t; \xi_s, kh), \eta(t; \xi_s, kh)]$. For small α, using the Taylor expansion we get $\xi(t; \xi_s, kh) = \xi_s + \alpha \Delta \xi + O(\alpha^2)$ and $\eta(t; \xi_s, kh) = kh + \alpha \Delta \eta + O(\alpha^2)$, where

$$\Delta \xi = -\beta J_w^{-1} x_\eta |_w \cos t, \quad \Delta \eta = \beta J_w^{-1} x_\xi |_w \cos t \tag{3.6a,b}$$

and

$$x_\xi |_w \equiv \partial x / \partial \xi |_{\eta=kh}, \quad x_\eta |_w \equiv \partial x / \partial \eta |_{\eta=kh}, \quad J_w \equiv \left(x_\xi |_w \right)^2 + \left(x_\eta |_w \right)^2. \tag{3.7a-c}$$

The derivatives of the transformation function are readily obtained from (2.7). More details can be found in appendix A. Using the Taylor expansions at $\widetilde{\eta} = \gamma$ (i.e. $\eta = kh$), we approximate (3.2a,b) as

$$\frac{\partial \psi}{\partial \xi} + \alpha \left[\frac{\partial^2 \psi}{\partial \xi \partial \widetilde{\eta}} \Delta \eta / \beta + \frac{\partial^2 \psi}{\partial \xi^2} \Delta \xi \right] + O(\alpha^2) = x_\xi |_w \sin t + O(\alpha \beta), \quad \text{at } \widetilde{\eta} = \gamma, \tag{3.8}$$

$$\frac{\partial \psi}{\partial \widetilde{\eta}} + \alpha \left[\frac{\partial^2 \psi}{\partial \widetilde{\eta}^2} \Delta \eta / \beta + \frac{\partial^2 \psi}{\partial \xi \partial \widetilde{\eta}} \Delta \xi \right] + O(\alpha^2) = \beta x_\eta |_w \sin t + O(\alpha \beta^2), \quad \text{at } \widetilde{\eta} = \gamma. \tag{3.9}$$

Assuming the perturbation expansion

$$\psi = \psi_0(\xi, \widetilde{\eta}, t) + \alpha \psi_1(\xi, \widetilde{\eta}, t) + \cdots \tag{3.10}$$

we obtain from (3.1), (3.3), (3.9) and (3.8) the approximate equations for the first two orders, as follows. At $O(\alpha^0)$,

$$\frac{\partial}{\partial t} \frac{\partial^2 \psi_0}{\partial \widetilde{\eta}^2} = \frac{1}{2} \sigma^2 J_0^{-1} \frac{\partial^4 \psi_0}{\partial \widetilde{\eta}^4}, \quad 0 < \widetilde{\eta} < \gamma, \tag{3.11}$$

$$\psi_0 = 0, \quad \frac{\partial^2 \psi_0}{\partial \widetilde{\eta}^2} = 0, \quad \text{at } \widetilde{\eta} = 0, \tag{3.12a,b}$$

$$\frac{\partial \psi_0}{\partial \xi} = x_\xi |_w \sin t, \quad \frac{\partial \psi_0}{\partial \widetilde{\eta}} = 0, \quad \text{at } \widetilde{\eta} = \gamma. \tag{3.13a,b}$$

At $O(\alpha)$,

$$\frac{\partial}{\partial t} \frac{\partial^2 \psi_1}{\partial \widetilde{\eta}^2} - \frac{\partial \left(\psi_0, \frac{1}{J_0} \frac{\partial^2 \psi_0}{\partial \widetilde{\eta}^2} \right)}{\partial \left(\xi, \widetilde{\eta} \right)} = \frac{1}{2} \sigma^2 J_0^{-1} \frac{\partial^4 \psi_1}{\partial \widetilde{\eta}^4}, \quad 0 < \widetilde{\eta} < \gamma, \tag{3.14}$$

$$\psi_1 = 0, \quad \frac{\partial^2 \psi_1}{\partial \widetilde{\eta}^2} = 0, \quad \text{at } \widetilde{\eta} = 0, \tag{3.15a,b}$$

$$\frac{\partial \psi_1}{\partial \xi} = -J_w^{-1} x_\xi|_w \frac{\partial^2 \psi_0}{\partial \xi \partial \widetilde{\eta}} \cos t, \quad \text{at } \widetilde{\eta} = \gamma, \tag{3.16}$$

$$\frac{\partial \psi_1}{\partial \widetilde{\eta}} = -J_w^{-1} x_\xi|_w \frac{\partial^2 \psi_0}{\partial \widetilde{\eta}^2} \cos t + \alpha^{-1} \beta x_\eta|_w \sin t, \quad \text{at } \widetilde{\eta} = \gamma. \tag{3.17}$$

It immediately follows from (3.13*b*) that $\partial^2 \psi_0 / \partial \xi \partial \widetilde{\eta} = 0$ at $\widetilde{\eta} = \gamma$, reducing (3.16) to

$$\frac{\partial \psi_1}{\partial \xi} = 0, \quad \text{at } \widetilde{\eta} = \gamma. \tag{3.18}$$

3.1. *The leading order solution*

To the lowest order approximation, the fluid flow is primarily driven by the wall velocity component normal to the corrugation surface, cf. (3.13*a*), as a result of the sawtooth slope being of $O(\beta)$. The solution is similar to that of an ordinary Stokes boundary layer, except for a parametric dependence on ξ, representing the effects of wall sawteeth. The solution is written as $\psi_0 = \widehat{\psi}_0(\xi, \widetilde{\eta}) e^{-it} + \text{c.c.}$, where

$$\widehat{\psi}_0(\xi, \widetilde{\eta}) = C(\xi) \left\{ \sinh \left[AF(\xi) \widetilde{\eta} \right] - \widetilde{\eta} AF(\xi) \cosh \left[AF(\xi) \gamma \right] \right\}, \tag{3.19}$$

$A \equiv (1 - i)\sigma^{-1}$, and $C(\xi)$ is to be determined. It can be readily checked that (3.19) satisfies (3.11), (3.12) and (3.13*b*). To satisfy (3.13*a*), $\partial \widehat{\psi}_0 / \partial \xi = (1/2) i x_\xi|_w$ at $\widetilde{\eta} = \gamma$, which upon integrating in ξ leads to

$$C(\xi) \left\{ \sinh \left[AF(\xi) \gamma \right] - AF(\xi) \gamma \cosh \left[AF(\xi) \gamma \right] \right\} = \tfrac{1}{2} i \left[x_w(\xi) + C_0 \right], \tag{3.20}$$

where $x_w(\xi) \equiv x(\xi, kh)$ using (2.7). The constant of integration C_0 is in general complex. Since $x_w(\xi)$ measures the distance in x following the corrugated wall, $C(\xi)$ is overall proportional to x. As the fluid is pushed in and out of the channel due to wall oscillations, the intensity of the flow field is expected to increase outwards from the channel centre towards the ends. This is similar to the boundary-layer solution when the channel walls are flat plates.

The arbitrary constant C_0 can be determined by imposing lateral boundary conditions at the channel ends. Consider a channel of finite length, whose two ends, $x = x_0$ and $x = x_1$, are submerged in reservoirs of the same fluid. Suppose the reservoirs are so large that no significant fluid motions are excited there, and have the same fluid levels so that there is zero imposed pressure difference. Thus, the dynamic pressure p at the two ends must vanish, i.e. $p = 0$ at $x = x_0, x_1$, or equivalently

$$\int_{x_0}^{x_1} \frac{\partial p}{\partial x} dx = 0, \quad \text{along } y = \text{constant}. \tag{3.21}$$

The condition of zero mean pressure drop has been similarly used in some previous studies on peristaltic transport (Yin & Fung 1971; Takagi & Balmforth 2011). The pressure gradient along channel is obtained from the momentum equation. Since the Stokes boundary layer follows the sawtooth profile, the pressure gradient $\partial p / \partial x$ varies
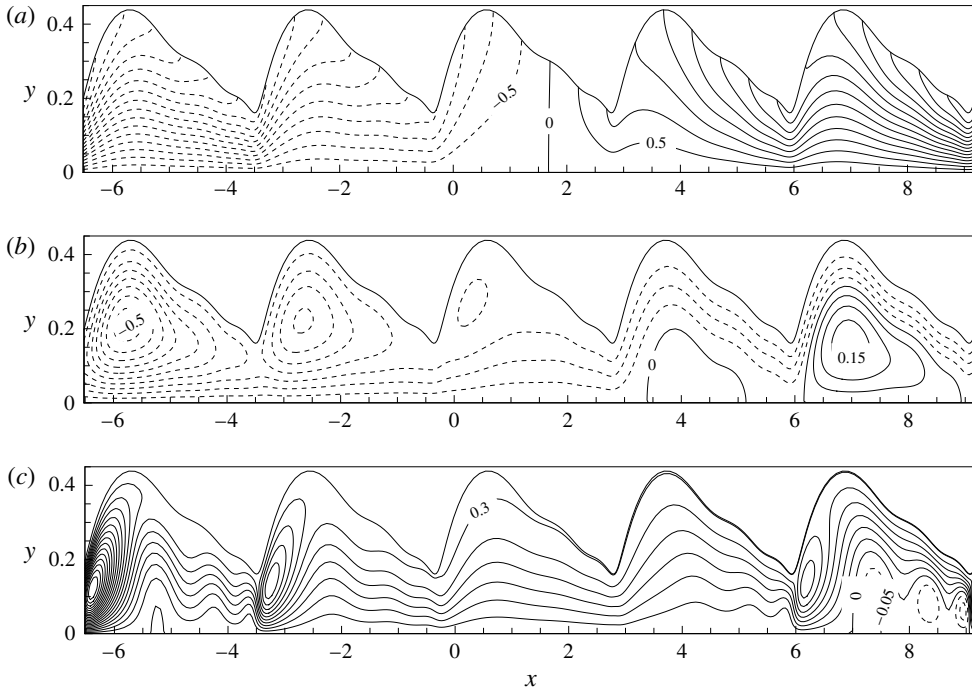
FIGURE 3. Contours of stream functions in the half plane $y > 0$ for an asymmetrical sawtooth wall profile: (*a*) the leading order flow ψ_0 at $t = \pi/2$, $\Delta\psi_0 = 0.5$, $-8.2228 \leqslant \psi_0 \leqslant 7.4852$; (*b*) ψ_0 at $t = \pi$ near the reversal of the flow, $\Delta\psi_0 = 0.05$, $-0.5268 \leqslant \psi_0 \leqslant 0.1813$; (*c*) the induced steady streaming $\alpha\psi_{10}$, $\alpha\Delta\psi_{10} = 0.05$, $-0.1250 \leqslant \psi_{10} \leqslant 1.0496$. Dashed lines indicate the negative contour values. Dimensionless parameters: oscillation amplitude $\alpha = 0.2$ and frequency $\sigma = 0.6538$, sawtooth wavelength $\beta = 0.3130$ and height $\epsilon_b = 1.0$.

both in x and y even at the leading order approximation. On the other hand, lines $y = $ constant $= \bar{y}$ are in general curves in the (ξ, η) plane. Thus, to carry out the integration in (3.21), one must invert the map (2.7) and (2.8), finding the curve in (ξ, η) that corresponds to $y = \bar{y}$. This is in general not convenient for an arbitrary choice of $\bar{y}$. However, the centreline $y = 0$ corresponds to $\eta = 0$, along which $\mathrm{d}x = x_\xi|_{\eta=0}\,\mathrm{d}\xi$. This greatly simplifies the work to deal with the pressure condition (3.21).

Upon integrating (3.21) along $\eta = 0$, we obtain the condition for determining the constant C_0, i.e.

$$C_0 \int_{\xi_0(0)}^{\xi_1(0)} \frac{\cosh{(AF\gamma)}}{\sinh{(AF\gamma)} - AF\gamma \cosh{(AF\gamma)}} \left.\frac{\partial x}{\partial \xi}\right|_{\eta=0} \mathrm{d}\xi$$

$$= -\int_{\xi_0(0)}^{\xi_1(0)} \frac{x_w(\xi)\cosh{(AF\gamma)}}{\sinh{(AF\gamma)} - AF\gamma \cosh{(AF\gamma)}} \left.\frac{\partial x}{\partial \xi}\right|_{\eta=0} \mathrm{d}\xi, \qquad (3.22)$$

where $\xi_0(0)$ and $\xi_1(0)$ correspond, respectively, to x_0 and x_1 at $\eta = 0$. For details, a reader is referred to appendix B. As an example, contours of stream function ψ_0 are shown in figure 3(*a,b*) at different phases of an oscillation cycle, for the sawtooth profile (dashed line) in figure 2. The increase of flow intensity towards the two ends of the channel is particularly noted. Near the time of flow reversal, vortices are formed

on the steeper sides of the teeth. Close to the channel ends, the vortices are strong, rotating in opposite senses.

3.2. *The rectified steady flow*

At $O(\alpha)$, the stream function $\psi_1 = \psi_{10} + (\widehat{\psi}_{11}e^{-it} + \widehat{\psi}_{12}e^{-2it} + \text{c.c.})$, in view of (3.14) and (3.17). The zeroth and second time harmonics, ψ_{10} and $\widehat{\psi}_{12}$, are induced by the nonlinear convective inertia of the vorticity, as well as its interaction with the wall movement. Owing to the sawtooth slope, the y velocity of wall motion has a component tangential to the corrugated surface. This is the source for $\widehat{\psi}_{11}$. The focus here is ψ_{10}, the induced steady streaming. From (3.14) to (3.18), the equations for ψ_{10} are written, as follows:

$$\frac{1}{2}\sigma^2\frac{\partial^4\psi_{10}}{\partial\widetilde{\eta}^4} = G(\xi, \widetilde{\eta}), \quad 0 < \widetilde{\eta} < \gamma, \tag{3.23}$$

$$\psi_{10} = 0, \quad \frac{\partial^2\psi_{10}}{\partial\widetilde{\eta}^2} = 0, \quad \text{at } \widetilde{\eta} = 0, \tag{3.24a,b}$$

$$\frac{\partial\psi_{10}}{\partial\widetilde{\eta}} = B(\xi), \quad \frac{\partial\psi_{10}}{\partial\xi} = 0 \quad \text{at } \widetilde{\eta} = \gamma, \tag{3.25a,b}$$

where

$$G(\xi, \widetilde{\eta}) = 2A\sigma^{-2}C^*C'F^3\left[2\cosh(A^*F\widetilde{\eta}) - \cosh(A^*F\gamma)\right]\sinh(AF\widetilde{\eta})$$
$$- 4i\sigma^{-4}F^4C\frac{d}{d\xi}\left[C^*\cosh(A^*F\gamma)\right]\widetilde{\eta}\cosh(AF\widetilde{\eta}) + \text{c.c.} \tag{3.26}$$

arises from the time average of nonlinear inertia, and

$$B(\xi) = -2\sigma^{-2}J_w^{-1}x_\xi|_w F^2\,\text{Im}\{C\sinh(AF\gamma)\}. \tag{3.27}$$

Here $*$ denotes the complex conjugate and $C' = dC/d\xi$. Owing to the viscosity, the fluid velocity near the wall has a phase shift with respect to the wall velocity. This leads to the correlation between $\partial^2\psi_0/\partial\widetilde{\eta}^2$ and the wall displacement $\Delta\eta$, which is the physical meaning of $B(\xi)$. Derivations of (3.26) and (3.27) are detailed in appendix C.

The solution, that satisfies (3.23) and (3.24), is

$$\psi_{10} = f_1(\xi)\sinh(2\sigma^{-1}F\widetilde{\eta}) + f_2(\xi)\sin(2\sigma^{-1}F\widetilde{\eta}) + f_3(\xi)\widetilde{\eta}\cosh(AF\widetilde{\eta})$$
$$+ f_4(\xi)\sinh(AF\widetilde{\eta}) + f_5(\xi)\widetilde{\eta}^3 + f_6(\xi)\widetilde{\eta} + \text{c.c.} \tag{3.28}$$

where

$$f_1(\xi) = \tfrac{1}{4}AF^{-1}C^*C', \tag{3.29a}$$

$$f_2(\xi) = -i\tfrac{1}{4}AF^{-1}C^*C', \tag{3.29b}$$

$$f_3(\xi) = 2i\sigma^{-2}C\frac{d}{d\xi}\left[C^*\cosh(A^*F\gamma)\right], \tag{3.29c}$$

$$f_4(\xi) = AF^{-1}\left\{C^*C'\cosh(A^*F\gamma) + 4C\frac{d}{d\xi}\left[C^*\cosh(A^*F\gamma)\right]\right\}, \tag{3.29d}$$

and f_5 and f_6 are to be determined by satisfying the wall boundary conditions. It follows from (3.25b) that $\psi_{10} = Q$ at $\widetilde{\eta} = \gamma$, where Q is an arbitrary constant,

indicating that the undisturbed channel wall position is effectively a streamline in the sense of time average. Thus, from (3.25*a,b*) we get

$$3\gamma^2 f_5(\xi) + f_6(\xi) + S_1(\xi) + \text{c.c.} = B(\xi), \tag{3.30}$$

$$\gamma^3 f_5 + \gamma f_6 + S_2(\xi) + \text{c.c.} = Q, \tag{3.31}$$

where

$$\begin{aligned} S_1(\xi) &= 2\sigma^{-1} F \left[f_1 \cosh\left(2\sigma^{-1} F\gamma\right) + f_2 \cos\left(2\sigma^{-1} F\gamma\right) \right] \\ &\quad + (f_3 + AF f_4) \cosh\left(AF\gamma\right) + AF\gamma f_3 \sinh\left(AF\gamma\right), \end{aligned} \tag{3.32}$$

$$\begin{aligned} S_2(\xi) &= f_1 \sinh\left(2\sigma^{-1} F\gamma\right) + f_2 \sin\left(2\sigma^{-1} F\gamma\right) \\ &\quad + f_3 \gamma \cosh\left(AF\gamma\right) + f_4 \sinh\left(AF\gamma\right). \end{aligned} \tag{3.33}$$

The physical interpretation of Q is as follows. The time-averaged volume flow rate through a cross-section of the channel is a constant, independent of x, as the fluid is incompressible. Denoting the time average by overlines, the net volume flow rate is

$$\overline{2\int_0^{y_s(x)+\alpha\beta\cos t} \frac{\partial\psi}{\partial y}\mathrm{d}y} = 2\overline{\psi|_{y_s(x)+\alpha\beta\cos t}} = 2\overline{\left(\psi + \alpha\beta\frac{\partial\psi}{\partial y}\cos t\right)}_{y=y_s(x)} + O(\alpha^2)$$

$$= 2\overline{\psi}_{y=y_s(x)} + O(\alpha^2) = 2\alpha Q + O(\alpha^2), \tag{3.34}$$

noting the boundary conditions (2.5*a*) and (2.6*a*). Thus, to the lowest order approximation $2\alpha Q$ represents the net volume flow rate averaged over one cycle, at which the fluid is pumped from one end to another through the channel. By satisfying the imposed condition of zero pressure drop between the channel ends, we obtain the condition for determining Q.

$$Q\int_{\xi_1(0)}^{\xi_2(0)} 3F^{-3} \left.\frac{\mathrm{d}x}{\mathrm{d}\xi}\right|_{\widetilde{\eta}=0} \mathrm{d}\xi = \int_{\xi_1(0)}^{\xi_2(0)} \left[S_3 + 3\gamma F^{-3} B\right] \left.\frac{\mathrm{d}x}{\mathrm{d}\xi}\right|_{\widetilde{\eta}=0} \mathrm{d}\xi, \tag{3.35}$$

where

$$S_3 = -\frac{4\gamma^3}{\sigma^4 F} C^* \cosh\left(AF\gamma\right) \frac{\mathrm{d}}{\mathrm{d}\xi}\left[C\cosh\left(AF\gamma\right)\right] + 3F^{-3}\left(S_2 - \gamma S_1\right) + \text{c.c.} \tag{3.36}$$

Algebraic details can be found in appendix B. Once Q is determined, f_5 and f_6 follow from (3.30) and (3.31), completing the solution ψ_{10}. The flow pattern of the induced steady streaming $\alpha\psi_{10}$ is shown in figure 3(*c*). The overall steady flow in the positive x direction is observed. Steady circulations of size smaller than sawtooth wavelength are seen to attach to the teeth, with their strengths increasing as we move toward the channel ends. The net transport of fluid in the $+x$ direction is at a rate $\alpha Q = 0.3037$ (over half channel width).

4. Results and discussions

It is here assumed that the channel length is an integer multiple of sawtooth wavelength, and we take the skewness parameter $0 \leqslant q \leqslant \pi/2$, so that the sawteeth are oriented as indicated in figure 2. The primary interest is the net transport of fluid, both the rate and direction, induced by the geometric asymmetry in the system.
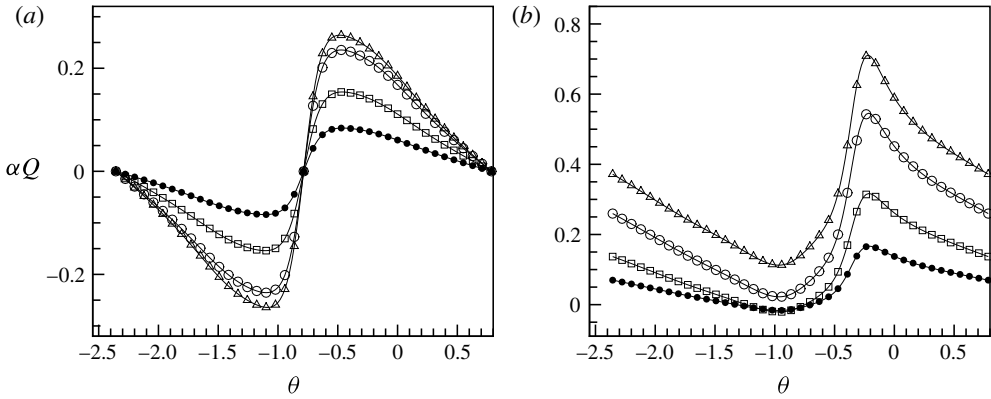
FIGURE 4. Time averaged volume flow rate αQ varying with phase angle θ which indicates the left end position: (*a*) symmetrical sawtooth with $q = 0.5\pi$. (*b*) Asymmetrical sawtooth with $q = 0.2\pi$. Parameters: oscillation amplitude $\alpha = 0.3$, sawtooth wavelength $\beta = 0.3130$ and height $\epsilon_b = 1.0$, and channel length $N\pi$, $N = 10$. Oscillation frequencies: $\triangle$, $\sigma = 0.6524$; $\bigcirc$, $\sigma = 0.8008$; $\square$, $\sigma = 1.1325$; $\bullet$, $\sigma = 1.6016$.

The left–right asymmetry is clearly introduced by the shape of the sawtooth provided $q \neq \pi/2$. However, even at $q = \pi/2$ with the sawteeth individually symmetrical, there is a second source of asymmetry due to the difference in the entrance and exit geometries at the channel ends, determined by their locations with respect to the phase of sawtooth wave. The fluid enters from both ends of the channel during the expansion half cycle of the oscillation and exits from both ends during the contraction half cycle. The entrance and exit flow conditions are influenced by the end geometries. As the flow intensity increases outward from the centre, cf. §3.1, the nonlinearity is expected to be the strongest near the channel ends. Both sources of asymmetry can lead to a rectified steady flow with a net directional transport of fluid. The effects due to both sources are, to some extent, independent but not exactly additive. We shall first clarify the effects of channel ends, then examine the net pumping rate in detail, focusing on the effects of sawtooth geometry.

4.1. *Effects of flow conditions at channel ends*

If the left end is taken at $x_0 + \theta$ (and the right end then at $N\pi + x_0 + \theta$), where θ measures the phase of a sawtooth wave, by varying θ over a range of π we cover all of the possibilities. Figure 4(*a*) shows the net pumping rate αQ varying with θ for a symmetrical sawtooth $q = \pi/2$. When the ends are located on a peak ($\theta = -\pi/4$) or trough ($\theta = -3\pi/4$, $\pi/4$) of the symmetrical sawtooth, the left–right symmetry is restored and αQ is identically zero, as expected; but for other locations, $\alpha Q \neq 0$. Here the net non-zero pumping can only be caused by the different geometries at the two channel ends. Figure 4(*b*) shows the case for an asymmetrical sawtooth with $q = 0.2\pi$. While these are similar to those in figure 4(*a*), note that the net pumping is mostly positive; slight negative pumping only occurs for large σ (low-frequency oscillation). This is generally found when asymmetrical sawteeth are oriented as in figure 2. As the oscillation frequency increases (σ decreases), the fluid velocity becomes greater, and so the nonlinearity is stronger. Effects of channel ends and sawtooth asymmetry are therefore both enhanced. In the case of symmetrical sawtooth, changing N does

not alter the graphs in figure 4(*a*). In the case of asymmetrical sawtooth, however, αQ changes in magnitude for different *N*; specifically, the positive pumping increases and the negative pumping decreases (in magnitude) with *N*, indicating the cumulative effects of sawteeth on breaking the left–right symmetry of the system. With $N = 1$ or 2 asymmetrical sawteeth, the negative minimum and positive maximum of the curve αQ versus θ are comparable in magnitude, with the latter being slightly greater.

The flow intensity increases towards the ends, overall proportional to the distance away from the channel centre, cf. §3.1. As the channel length is increased, the flow velocity and vortex activity become stronger, producing a greater difference between the flow conditions at the two ends, if a difference in the end geometries is present. On the other hand, the total wall friction is also greater for longer channels. In the absence of sawtooth asymmetry, a state of rectified steady flow is established which provides an overall viscous friction necessary to balance the effects of channel ends such that the mean pressure drop is zero (as imposed). The volume flow rate of this steady state, a manifestation of the spatially averaged velocity, is invariant to the length *N*, given the end geometries and oscillation conditions. As a loose comparison, this is analogous to the problem of a thin layer of viscous fluid on a slope, in which the gravity–friction balanced steady flow is independent of the length of the slope. The cumulative effects of sawtooth asymmetry are anticipated, and discussed in the section that follows.

The flow patterns of the induced streaming ψ_{10} are shown in figure 5 for the case of symmetrical sawtooth, using different end positions. For $\theta = -\pi/4$ in figure 5(*b*), both ends are at a peak, and the flow is left–right antisymmetric, having zero spatial average. The end positions corresponding to the negative minimum and positive maximum pumping rate in figure 4(*a*) are exactly the mirror reflection of each other, and so are the flow patterns, cf. figure 5(*a*,*c*). It is found that the effects of entrance and flow conditions in general induce a net pumping directed towards the end that is closer to a sawtooth peak. Because the sawtooth height is large, the local channel width at a sawtooth peak is much smaller than that at a trough. Therefore, a small change in the phase θ near a sawtooth peak results in a larger relative change in the local channel width than a similar change of θ near a trough. This perhaps is the reason that the location of a peak is more sensitive in determining the direction of net pumping caused by the end flow conditions. It also explains the sharp variation in αQ between the positions θ corresponding to the negative minimum and positive maximum αQ.

4.2. *Net pumping rate*

In the discussion that follows, the channel ends have been placed at or near the positions corresponding to the maximum αQ in figure 4(*b*). The entrance and exit geometries at the channel ends are the same as indicated in figure figure 3.

Given a sawtooth profile and oscillation amplitude, the net pumping rate αQ increases rapidly as σ decreases (i.e. as the oscillation frequency increases or the fluid viscosity decreases), as shown in figure 6(*a*). The rate of increase is approximately exponential. Holding σ fixed, the pumping rate increases linearly with the oscillation amplitude α, cf. figure 6(*b*), with the slope of the linear lines being *Q* and increasing with *N*. From (3.35), *Q* is a function of channel length *N*, frequency σ and sawtooth geometry. Noting that *a* appears in the normalization for ψ, cf. (2.2), the dimensional pumping rate increases quadratically with oscillation amplitude. It is clear from figure 6 that the channel length, in terms of the number *N* of sawteeth, has strong influence on the net pumping, in particular for oscillations at high frequencies and large amplitudes.
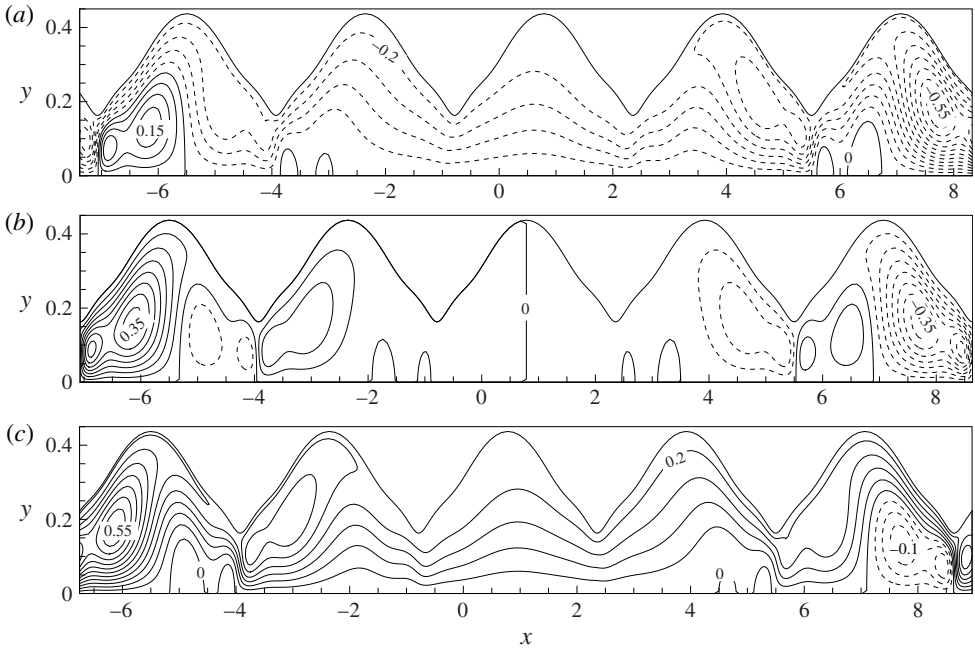
FIGURE 5. Contours of the stream function $\alpha\psi_{10}$ for a symmetrical sawtooth wall profile. The left end position: (*a*) $\theta = -1.0996$, $-0.5933 \leqslant \alpha\psi_{10} \leqslant 0.1958$ and $\alpha Q = -0.2355$; (*b*) $\theta = -0.7854$ (i.e. $-\pi/4$), $-0.3773 \leqslant \alpha\psi_{10} \leqslant 0.3773$ and $\alpha Q = 0.0$; (*c*) $\theta = -0.4712$, $-0.1958 \leqslant \alpha\psi_{10} \leqslant 0.5933$ and $\alpha Q = 0.2355$. The contour increment $\alpha\Delta\psi_{10} = 0.05$. Parameters: oscillation amplitude $\alpha = 0.3$ and frequency $\sigma = 0.8008$, sawtooth wavelength $\beta = 0.3130$ and height $\epsilon_b = 1.0$, and $N = 5$ for the channel length.
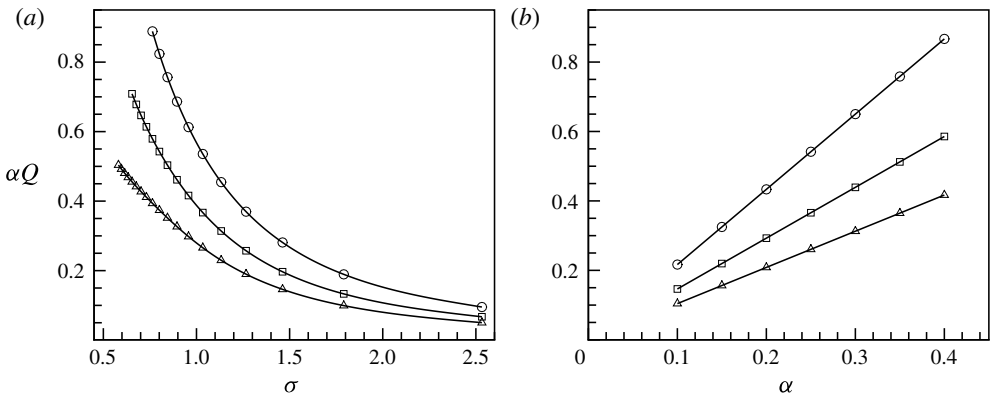

FIGURE 6. Effects of oscillation on the net pumping rate αQ (for half channel width) for an asymmetry sawtooth with $q = 0.2\pi$, wavelength $\beta = 0.3130$ and height $\epsilon_b = 1.0$: (*a*) αQ versus oscillation frequency σ for amplitude $\alpha = 0.3$; (*b*) αQ versus α for $\sigma = 0.9247$. For channel lengths: $\bigcirc$, $N = 15$; $\square$, $N = 10$; $\triangle$, $N = 5$.
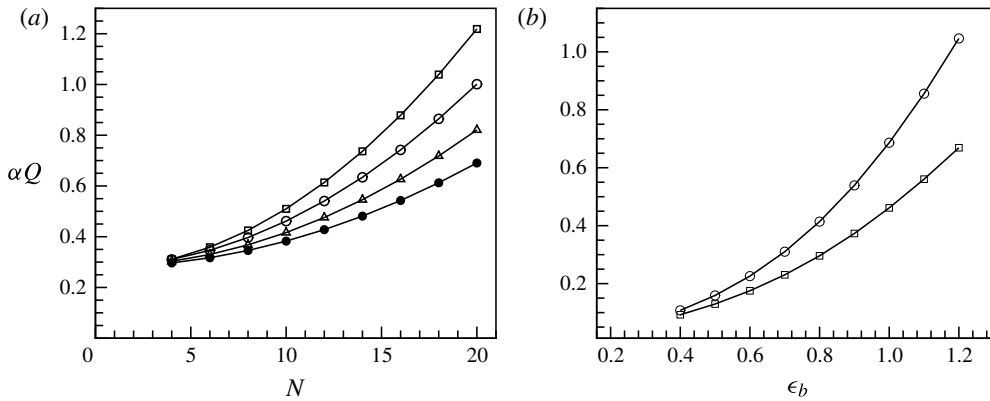
FIGURE 7. Effects of sawtooth geometry on the net pumping rate αQ (for half channel width) for oscillation amplitude $\alpha = 0.3$ and frequency $\sigma = 0.8953$. (*a*) Plots of αQ versus N. Sawtooth height $\epsilon_b = 1.0$, and wavelengths: ●, $\beta = 0.2090$ ($\lambda_s \simeq 15h_0$); △, $\beta = 0.2506$ ($\lambda_s \simeq 12.5h_0$); ○, $\beta = 0.3130$ ($\lambda_s \simeq 10h_0$); □, $\beta = 0.4166$ ($\lambda_s \simeq 7.5h_0$). (*b*) Plots of αQ versus ϵ_b for $\beta \simeq 0.31$: ○, $N = 15$; □, $N = 10$. The skewness parameter for the sawtooth $q = 0.2\pi$.

The cumulative effect of sawteeth is illustrated in figure 7(*a*), in which αQ increases with N, fixing all other parameters. The curves match with polynomial fitting of order two. When we reduce β, holding ϵ_b fixed, we effectively make the sawtooth more gently sloped while keeping the same sawtooth height relative to the channel width. As a result, αQ decreases. For sufficiently small N, the effects of sawtooth asymmetry on the flow cannot be fully developed during any half cycle of an oscillation due to the short channel length, and are reversed during the other half of the cycle as the flow directions are reversed. Thus, the sawtooth asymmetry is insufficient to produce a net transport of fluid when there are only a few sawteeth in the channel. In such a case, the net pumping rate αQ is dominantly influenced by the entrance and exit flow conditions at the channel ends. This expectation is confirmed by the result in figure 7(*a*) that αQ becomes independent of β as N is reduced while keeping the end positions fixed with respect to the phase of the sawtooth wave. Given an oscillation condition, αQ increases with the sawtooth height ϵ_b, following a polynomial fitting of order four within the range of ϵ_b explored, cf. figure 7(*b*). We note that β varies slightly from 0.3141 to 0.3120, as we fix the sawtooth wavelength while increasing the height ϵ_b from 0.4 to 1.2. This is due to the fact that we choose the map and adapt the wall geometry subsequently.

To fix the idea, let us take for example the sawtooth wavelength $\lambda_s = 5$ mm. For the sawtooth profile (dashed curve) in figure 2, $\beta = 0.3130$ and $\epsilon_b = 1.0$ correspond to a half channel width $h_0 = 0.4982$ mm and sawtooth height $h_s = 0.4650$ mm. For water, $\nu = 1$ mm^2 s^{-1}. From figure 6(*a*), $\alpha Q = 0.6863$ for $\alpha = 0.3$, $\sigma = 0.8953$, $N = 15$. Thus, in a channel of length 75 mm, when the sawtooth channel walls oscillate at an amplitude $a = 0.1495$ mm and frequency $f = 1.60$ Hz, the fluid is pumped in the $+x$ direction at a rate $2 \times (\alpha Q)a\omega k^{-1} = 197.0$ μL min^{-1}mm^{-1} wall width. If the sawtooth wavelength is increased to $\lambda_s = 10$ mm, subsequently the half channel width $h_0 = 0.9964$ mm and sawtooth height $h_s = 0.930$ mm. With the oscillation amplitude of 0.2990 mm but frequency of 0.4 Hz (keeping $\sigma = 0.8953$), the same pumping rate can be achieved in a channel of length 150 mm. Similarly, we can also reinterpret

the case by taking $\lambda_s = 2.5$ mm and reducing all other lengths by a factor of two but increasing the frequency to $f = 6.4$ Hz.

In view of the discussion in § 4.1, the effects of entrance and exit flow conditions have minimum contribution to the net directional pumping when both ends are placed at a sawtooth peak or trough. On the other hand, to maximize the net pumping in the positive x direction for the sawteeth oriented as indicated in figure 2, it is in one's interest to keep a peak closer to the right end from inside the channel. Starting with the end positions as indicated in figure 3 which give the maximum positive αQ seen in figure 4(*b*), if the right end is moved outward (corresponding to increasing θ), the pumping rate tends to be reduced but still positive; however, if the right end is moved inward (corresponding to decreasing θ), αQ decreases rapidly and could even become negative depending on σ, as the sawtooth peak previously close to the right end is disappearing from the channel and a sawtooth peak appears at the left end. The effects of ends is less important for long channels in which the pumping rate and direction are primarily determined by the effects of sawtooth asymmetry. However, very long channels may not be of practical interest considering the power that is needed to vibrate the channel walls against incompressible fluids.

At the time of writing, the experimental results referred to Thiria & Zhang (2010) have not been published. While the pumping direction is not explicitly noted in the report, a reference in Dupeux *et al.* (2011) indicates that the net transport of fluid in Thiria & Zhang's experiment is in the $+x$ direction if the sawteeth are oriented as in figure 2. A private communication with Professor R. Camassa seems to confirm the author's interpretation of the pumping direction in the experiment.

4.3. *Power input and rate of viscous dissipation*

To the lowest order approximation, the rate $\dot{W}$ at which the work is delivered to the channel wall from outside means is

$$\dot{W} = \frac{1}{2\pi} \int_{x_0}^{x_1} \int_0^{2\pi} (p_0 - \tau_{ny}) \sin t \, dt \, dx, \quad \text{along } y = y_s(x), \quad (4.1)$$

averaged over the period of oscillation. Here τ_{ny} is the y component of the normal stress at the wall. When the channel walls are flat plates, $\tau_{ny} = \tau_{yy} = 0$. Since there is zero mean pressure drop between the channel ends, the rate at which the useful energy is stored in the fluid is identically zero. Thus, the rate of work delivered to the channel wall must be balanced entirely by the rate of viscous dissipation $\dot{D}$ in the fluid,

$$\dot{D} = \frac{1}{2}\sigma^2\beta^2 \int_{x_0}^{x_1} \int_0^{y=y_s(x)} \left[2\left(\frac{\partial u_0}{\partial x}\right)^2 + 2\left(\frac{\partial v_0}{\partial y}\right)^2 + \left(\frac{\partial u_0}{\partial y} + \frac{\partial v_0}{\partial x}\right)^2 \right] dy \, dx. \quad (4.2)$$

This situation, $\dot{W} = \dot{D}$, similarly occurs in Takagi & Balmforth (2011), in which pumping of viscous fluid is induced by steady peristaltic waves propagating down an elastic tube. In those cases, the mechanical efficiency based on the rate of useful energy stored in the fluid (flow rate × pressure drop against pumping) as in Shapiro, Jaffrin & Weinberg (1969), is zero. Takagi & Balmforth defined an alternative pumping efficiency which measures the fluid transport per unit input power. (This definition does not have the appropriate dimensions for efficiency.) The concern, of course, is a different one from that in fluid machinery. Here the question is how

much energy is needed to achieve a desired transport of fluid, rather than the energy efficiency of the transport mechanism.

The calculation of $\dot{D}$, or $\dot{W}$ can be carried out using the solution in §3.1, but it is unavoidably tedious, attainable only by numerical evaluations because of the wall geometry. In an averaged sense, it is reasonable to expect that $\dot{W}$ could be characterized by $\dot{W}_f$ for flat channel walls with same oscillation frequency and amplitude, but with a channel width kh seen in the mapped plane to account for the effects of sawtooth shape and height. For simple purposes and an order of magnitude estimate, this may be useful. The analytical expression for $\dot{W}_f$ is derived in appendix D, for the benefits of readers who may be interested.

5. Concluding remarks

We have developed a theory describing the effects of ratcheting fluid in a narrow channel between two facing sawtooth walls that undergo harmonic oscillations opposing each other and normal to the channel centreline. Among the assumptions of our theory are that the periodic sawtooth geometry has a large peak-to-trough height and long wavelength, compared with the mean channel width, and the oscillations are of small amplitude and moderate frequency.

A 'terrain-following' boundary-layer approach is formulated using a conformal transformation. The analytical solutions are given for the induced steady flow field and net pumping rate of fluid. The rectification of time harmonic motion is seen due to (i) the steady momentum flux that arises from the nonlinear convective inertia of the oscillating flow, and (ii) the interaction of vorticity with the wall motion, that arises due to the fluid velocity near the wall being out of phase with the wall velocity, as a result of viscosity. The geometric asymmetry renders these effects to be spatially biased, leading to a unidirectional component in the steady flow. Effects on the net pumping rate have been examined varying parameters representing oscillation conditions and sawtooth geometry. We have also clarified the effects of entrance and exit flow conditions due to the geometries at channel ends. This is a secondary source of spatial asymmetry in the system, and can cause a net directional pumping even when the sawteeth are individually symmetrical. Whereas the influences from both sources of symmetry-breaking can be comparable in a short channel with a few sawteeth, the accumulative effects of asymmetric wall profile become dominant as the number of sawteeth increases, determining the net pumping (rate and direction) of fluid in a long channel.

This work is a demonstration of judicious use of the conformal transformation method, which was developed for potential flows in finite domains (Yu & Howard 2012), to study the vorticity dynamics. Here, a boundary-layer approximation is invoked for the sake of obtaining an analytical solution. This can be relaxed if numerical solutions are sought. The mapping functions can also be adapted to be time-dependent to consider large-amplitude wall oscillations, providing an alternative in numerical modeling of flows with complex boundary geometry.

Acknowledgements

Appendix A. The instantaneous wall position

Consider a point (x, y) on the channel wall at a time t. In a small time interval δt, it is displaced to $(x, y + \delta y)$, where $\delta y = -(\alpha\beta \sin t)\,\delta t$. In the mapped plane, this point is displaced from (ξ, η) to $(\xi + \delta\xi, \eta + \delta\eta)$, where

$$0 = \frac{\partial x}{\partial \xi}\delta\xi + \frac{\partial x}{\partial \eta}\delta\eta, \quad \delta y = \frac{\partial y}{\partial \xi}\delta\xi + \frac{\partial y}{\partial \eta}\delta\eta. \qquad (A\,1a,b)$$

Solving for $\delta\xi$ and $\delta\eta$, and in the limit as $\delta t \to 0$, we obtain a pair of parametric equations

$$\frac{\mathrm{d}\xi}{\mathrm{d}t} = \alpha\beta \frac{1}{J}\frac{\partial x}{\partial \eta}\sin t, \quad \frac{\mathrm{d}\eta}{\mathrm{d}t} = -\alpha\beta \frac{1}{J}\frac{\partial x}{\partial \xi}\sin t, \qquad (A\,2a,b)$$

describing the trajectory of a point on the channel wall. From the instantaneous positions of these points, the wall position $\eta = \eta_{sw}(\xi, t)$ is found. In general, (A 2) cannot be integrated analytically, as the right-hand side functions are highly nonlinear in t.

Let us identify the points forming the corrugated surface by their undisturbed positions (ξ_s, kh). Their positions at time t are $[\xi(t; \xi_s, kh), \eta(t; \xi_s, kh)]$. The displacement of a point from its original position is

$$\left(\alpha\beta \int_0^t \frac{1}{J}\frac{\partial x}{\partial \eta}\sin t\,\mathrm{d}t, \quad -\alpha\beta \int_0^t \frac{1}{J}\frac{\partial x}{\partial \xi}\sin t\,\mathrm{d}t \right), \qquad (A\,3)$$

where the integrands are to be evaluated at the instantaneous position (ξ, η). For small-amplitude oscillations, the displacement is of $O(\alpha) \ll 1$, and we can therefore approximate the integrands above using Taylor expansions at the mean position (ξ_s, kh), obtaining

$$\xi(t; \xi_s, kh) - \xi_s = -\alpha\beta \left[\frac{1}{J}\frac{\partial x}{\partial \eta} \right]_{(\xi_s,kh)} \cos t + O(\alpha^2), \qquad (A\,4)$$

$$\eta(t; \xi_s, kh) - kh = \alpha\beta \left[\frac{1}{J}\frac{\partial x}{\partial \xi} \right]_{(\xi_s,kh)} \cos t + O(\alpha^2). \qquad (A\,5)$$

These give the expressions in (3.6) where the subscript w indicates the evaluation of functions at $\eta = kh$ for a given ξ_s.

Appendix B. The pressure gradient along channel

Let the dynamic pressure be normalized as $p = p'/(\rho a \omega^2 k^{-1})$. The dimensionless momentum equation along channel is

$$\frac{\partial}{\partial t}\frac{\partial \psi}{\partial y} - \alpha\beta \frac{\partial\left(\psi, \dfrac{\partial\psi}{\partial y}\right)}{\partial(x,y)} = -\frac{\partial p}{\partial x} + \frac{1}{2}\sigma^2\beta^2\nabla_{xy}^2\frac{\partial\psi}{\partial y}, \qquad (B\,1)$$

where

$$\nabla_{xy}^2 = \frac{\partial^2}{\partial x^2} + \frac{\partial^2}{\partial y^2}. \qquad (B\,2)$$

Under the conformal transformation, $\nabla^2_{xy} = J^{-1}\nabla^2$, where ∇^2 is the Laplacian operator in the mapped plane, cf. (2.13). For any functions A and B

$$\frac{\partial (A, B)}{\partial (x, y)} = \frac{\partial (A, B)}{\partial (\xi, \eta)}\frac{\partial (\xi, \eta)}{\partial (x, y)} = J^{-1}\frac{\partial (A, B)}{\partial (\xi, \eta)}. \tag{B 3}$$

Form (2.15),

$$\frac{\partial \psi}{\partial y} = J^{-1}\Psi, \quad \Psi \equiv \frac{\partial \psi}{\partial \eta}\frac{\partial x}{\partial \xi} - \frac{\partial \psi}{\partial \xi}\frac{\partial x}{\partial \eta}. \tag{B 4}$$

Thus, in terms of ξ and η, equation (B 1) is written as

$$\frac{\partial p}{\partial x} = -\frac{1}{J}\frac{\partial \Psi}{\partial t} + \alpha\beta\frac{1}{J}\frac{\partial \left(\psi, J^{-1}\Psi\right)}{\partial (\xi, \eta)} + \sigma^2\beta^2\frac{1}{2J}\nabla^2\left(J^{-1}\Psi\right). \tag{B 5}$$

Upon rescaling $\widetilde{\eta} = \eta/\beta$, it becomes

$$\beta\frac{\partial p}{\partial x} = -\frac{1}{J}\frac{\partial \widetilde{\Psi}}{\partial t} + \alpha\frac{1}{J}\frac{\partial \left(\psi, J^{-1}\widetilde{\Psi}\right)}{\partial \left(\xi, \widetilde{\eta}\right)} + \sigma^2\frac{1}{2J}\widetilde{\nabla}^2\left(J^{-1}\widetilde{\Psi}\right), \tag{B 6}$$

where

$$\widetilde{\Psi} \equiv \frac{\partial \psi}{\partial \widetilde{\eta}}\frac{\partial x}{\partial \xi} - \beta\frac{\partial \psi}{\partial \xi}\frac{\partial x}{\partial \eta}, \tag{B 7}$$

and $\widetilde{\nabla}^2$ is defined in (3.4). Note that $x(\xi, \eta)$ and J are known functions and not rescaled. Recall that for $\beta \ll 1$, $J(\xi, \eta) = J_0(\xi) + O(\beta^2)$, $\partial x/\partial \xi = F(\xi) + O(\beta^2)$, and $\partial x/\partial \eta = O(\beta)$, cf. (3.5), (2.7) and (2.8). Since $O(\beta) = O(\alpha)$, the appropriate expansion for pressure is $p = \alpha^{-1}p_0 + p_1 + \alpha p_2 \ldots$. Inserting into (B 6) and using the expansion (3.10) for ψ, we collect the equations for the first two orders. At $O(\alpha^{-1})$,

$$\beta\alpha^{-1}\frac{\partial p_0}{\partial x} = -F^{-1}\frac{\partial}{\partial t}\frac{\partial \psi_0}{\partial \widetilde{\eta}} + \frac{1}{2}\sigma^2 F^{-3}\frac{\partial^3\psi_0}{\partial \widetilde{\eta}^3}, \tag{B 8}$$

and at $O(\alpha^0)$,

$$\beta\frac{\partial p_1}{\partial x} = -\alpha F^{-1}\frac{\partial}{\partial t}\frac{\partial \psi_1}{\partial \widetilde{\eta}} + \frac{1}{2}\alpha\sigma^2 F^{-3}\frac{\partial^3\psi_1}{\partial \widetilde{\eta}^3}$$
$$+ \alpha\left[F^{-3}\frac{\partial \psi_0}{\partial \xi}\frac{\partial^2\psi_0}{\partial \widetilde{\eta}^2} - F^{-2}\frac{\partial \psi_0}{\partial \widetilde{\eta}}\frac{\partial}{\partial \xi}\left(F^{-1}\frac{\partial \psi_0}{\partial \widetilde{\eta}}\right)\right]. \tag{B 9}$$

At the leading order $p_0 = \widehat{p}_0 e^{-it} + \text{c.c.}$ From (3.19),

$$\frac{\partial \widehat{\psi}_0}{\partial \widetilde{\eta}} = CAF\left[\cosh(AF\widetilde{\eta}) - \cosh(AF\gamma)\right] \tag{B 10a}$$

$$\frac{\partial^2 \widehat{\psi}_0}{\partial \widetilde{\eta}^2} = C(AF)^2\sinh(AF\widetilde{\eta}) \tag{B 10b}$$

$$\frac{\partial^3 \widehat{\psi}_0}{\partial \widetilde{\eta}^3} = C(AF)^3\cosh(AF\widetilde{\eta}) \tag{B 10c}$$

$$\frac{\partial \widehat{\psi}_0}{\partial \xi} = C' \left[\sinh (AF\widetilde{\eta}) - \widetilde{\eta} AF \cosh (AF\gamma) \right]$$

$$+ CAF'\widetilde{\eta} \left[\cosh (AF\widetilde{\eta}) - \cosh (AF\gamma) - AF\gamma \sinh (AF\gamma) \right]. \quad (B\,10d)$$

Substituting into (B 8) and noting that $A^2 = -2\mathrm{i}\sigma^{-2}$, we get

$$\beta\alpha^{-1} \frac{\partial \widehat{p}_0}{\partial x} = -\mathrm{i} CA \cosh (AF\gamma). \quad (B\,11)$$

Although it appears to depend only on ξ when expressed in terms of the mapped variables, $\partial \widehat{p}_0 / \partial x$ in fact varies both in x and y, as lines of $\xi = \text{constant}$ correspond to curves in the (x, y) plane. In the pressure condition (3.21), the integration has to be done along $y = \text{constant} = \bar{y}$, given the definition of partial derivatives in x. We could carry out this integration in function of x or transform it to function of ξ. In either case, we have to invert the map (2.7) and (2.8), finding the curve in (ξ, η) that corresponds to $y = \bar{y}$. This is in general not convenient for an arbitrary choice of $\bar{y}$. However, the centreline $y = 0$ corresponds to $\eta = 0$, along which $\mathrm{d}x = x_\xi|_{\eta=0}\,\mathrm{d}\xi$. Thus, using C in (3.20), we integrate (B 11) along $\eta = 0$. Upon requiring the pressure difference to vanish, we obtain the condition for determining the constant C_0, as in (3.22).

Let $p_1 = p_{10} + \widehat{p}_{11}\mathrm{e}^{-\mathrm{i}t} + \widehat{p}_{12}\mathrm{e}^{-2\mathrm{i}t} + \text{c.c.}$ From (B 9), the equation for steady-state pressure p_{10} is written as

$$\beta\alpha^{-1} \frac{\partial p_{10}}{\partial x} = \frac{1}{2}\sigma^2 F^{-3} \frac{\partial^3 \psi_{10}}{\partial \widetilde{\eta}^3} + F^{-3} \left[\frac{\partial \widehat{\psi}_0}{\partial \xi} \frac{\partial^2 \widehat{\psi}_0^*}{\partial \widetilde{\eta}^2} - F \frac{\partial \widehat{\psi}_0^*}{\partial \widetilde{\eta}} \frac{\partial}{\partial \xi} \left(\frac{1}{F} \frac{\partial \psi_0}{\partial \widetilde{\eta}} \right) + \text{c.c.} \right]. \quad (B\,12)$$

The condition of zero pressure drop means $p_{10} = 0$ at $x = x_0, x_1$, i.e.

$$\int_{x_0}^{x_1} \left. \frac{\partial p_{10}}{\partial x} \right|_{y=0} \mathrm{d}x = \int_{\xi_0(0)}^{\xi_1(0)} \left[\frac{\partial p_{10}}{\partial x} \frac{\partial x}{\partial \xi} \right]_{\eta=0} \mathrm{d}\xi = 0, \quad (B\,13)$$

following (3.21). From (B 10b) and (B 10d), $\partial \widehat{\psi}_0 / \partial \xi = \partial^2 \widehat{\psi}_0 / \partial \widetilde{\eta}^2 = 0$ at $\widetilde{\eta} = 0$. Thus, for the nonlinear terms inside the square brackets in (B 12), we only need

$$-\frac{\partial \widehat{\psi}_0^*}{\partial \widetilde{\eta}} \frac{\partial}{\partial \xi} \left(\frac{1}{F} \frac{\partial \psi_0}{\partial \widetilde{\eta}} \right) = -\frac{2}{\sigma^2} C^* F \left[1 - \cosh (A^* F\gamma) \right] \left\{ C' - \frac{\mathrm{d}}{\mathrm{d}\xi} \left[C \cosh (AF\gamma) \right] \right\} \quad (B\,14)$$

at $\widetilde{\eta} = 0$. From (3.28),

$$\frac{\partial^3 \psi_{10}}{\partial \widetilde{\eta}^3} = \frac{8}{\sigma^3} F^3 \left[f_1 \cosh (2\sigma^{-1} F\widetilde{\eta}) - f_2 \cos (2\sigma^{-1} F\widetilde{\eta}) \right] + 3f_3 (AF)^2 \cosh (AF\widetilde{\eta})$$

$$+ f_3 \widetilde{\eta} (AF)^3 \sinh (AF\widetilde{\eta}) + f_4 (AF)^3 \cosh (AF\widetilde{\eta}) + 6f_5 + \text{c.c.} \quad (B\,15)$$

hence at $\widetilde{\eta} = 0$,

$$\frac{1}{2}\sigma^2 F^{-3} \frac{\partial^3 \psi_{10}}{\partial \widetilde{\eta}^3} = 4\sigma^{-1}(f_1 - f_2) - 3\mathrm{i}F^{-1}f_3 - \mathrm{i}Af_4 + 3\sigma^2 F^{-3}f_5 + \text{c.c.} \quad (B\,16)$$

From (3.30) and (3.31),

$$2\gamma^3 f_5 = \gamma B + (S_2 - \gamma S_1 + \text{c.c.}) - Q. \quad (B\,17)$$

Putting together (B 14), (B 16) and (B 17), and inserting into (B 12), we get, after some algebra, at $\widetilde{\eta} = 0$

$$
\begin{aligned}
\beta\alpha^{-1}\frac{\partial p_{10}}{\partial x} = {} & \frac{3\sigma^2}{2\gamma^3 F^3}\left[S_2 - \gamma S_1 + \text{c.c.} + \gamma B - Q\right] \\
& - \frac{2}{\sigma^2 F}C^*\cosh\left(A^*F\gamma\right)\frac{\mathrm{d}}{\mathrm{d}\xi}\left[C\cosh\left(AF\gamma\right)\right] + \text{c.c.} \\
& - \frac{2}{\sigma^2 F}\left\{C^*\frac{\mathrm{d}}{\mathrm{d}\xi}\left[C\cosh\left(AF\gamma\right)\right] - C\frac{\mathrm{d}}{\mathrm{d}\xi}\left[C^*\cosh\left(A^*F\gamma\right)\right]\right\} + \text{c.c.}
\end{aligned}
$$
(B 18)

Note that the terms in the curl brackets above are pure imaginary, hence cancel out with their complex conjugates. Substituting into (B 13), we get the condition for determining Q as in (3.35).

Appendix C. The derivations of G and B

The forcing for ψ_{10} in (3.23) is

$$
G(\xi, \widetilde{\eta}) = -\frac{\partial\widehat{\psi}_0}{\partial\xi}\frac{\partial^3\widehat{\psi}_0^*}{\partial\widetilde{\eta}^3} + J_0\frac{\partial\widehat{\psi}_0^*}{\partial\widetilde{\eta}}\frac{\partial}{\partial\xi}\left(\frac{1}{J_0}\frac{\partial^2\widehat{\psi}_0}{\partial\widetilde{\eta}^2}\right) + \text{c.c.} \equiv I_1 + I_2.
$$
(C 1)

Using the derivatives in (B 10),

$$
\begin{aligned}
I_1 = {} & -\frac{\partial\widehat{\psi}_0}{\partial\xi}\frac{\partial^3\widehat{\psi}_0^*}{\partial\widetilde{\eta}^3} + \text{c.c.} \\
= {} & \left\{C'\left[\widetilde{\eta}AF\cosh\left(AF\gamma\right) - \sinh\left(AF\widetilde{\eta}\right)\right] + CAF'\widetilde{\eta}\left[AF\gamma\sinh\left(AF\gamma\right)\right.\right. \\
& \left.\left. + \cosh\left(AF\gamma\right) - \cosh\left(AF\widetilde{\eta}\right)\right]\right\}A^{*3}F^3C^*\cosh\left(A^*F\widetilde{\eta}\right) + \text{c.c.} \\
= {} & 4\mathrm{i}\sigma^{-4}C^*F^3\widetilde{\eta}\cosh\left(A^*F\widetilde{\eta}\right)\left[(CF)'\cosh\left(AF\gamma\right) + CFAF'\gamma\sinh\left(AF\gamma\right)\right] \\
& + 2\sigma^{-2}AC^*C'F^3\sinh\left(AF\widetilde{\eta}\right)\cosh\left(A^*F\widetilde{\eta}\right) + \text{c.c.}
\end{aligned}
$$
(C 2)

In the above derivation, the terms associated with $\widetilde{\eta}\cosh\left(AF\widetilde{\eta}\right)\cosh\left(A^*F\widetilde{\eta}\right)$ are pure imaginary, hence have no contribution to I_1. Note that $\mathrm{i}A = A^*$, and $J_0 = F^2$, cf. (3.5). Thus,

$$
\frac{\partial}{\partial\xi}\left(\frac{1}{J_0}\frac{\partial^2\widehat{\psi}_0}{\partial\widetilde{\eta}^2}\right) = -2\mathrm{i}\sigma^{-2}\frac{\mathrm{d}}{\mathrm{d}\xi}\left[C\sinh\left(AF\widetilde{\eta}\right)\right]
$$
(C 3)

and

$$
\begin{aligned}
I_2 = {} & J_0\frac{\partial\widehat{\psi}_0^*}{\partial\widetilde{\eta}}\frac{\partial}{\partial\xi}\left(\frac{1}{J_0}\frac{\partial^2\widehat{\psi}_0}{\partial\widetilde{\eta}^2}\right) + \text{c.c.} \\
= {} & -2\mathrm{i}\sigma^{-2}C^*A^*F^3\left[\cosh\left(A^*F\widetilde{\eta}\right) - \cosh\left(A^*F\gamma\right)\right]\frac{\mathrm{d}}{\mathrm{d}\xi}\left[C\sinh\left(AF\widetilde{\eta}\right)\right] + \text{c.c.} \\
= {} & 2\sigma^{-2}AF^3C^*C'\left[\cosh\left(A^*F\widetilde{\eta}\right) - \cosh\left(A^*F\gamma\right)\right]\sinh\left(AF\widetilde{\eta}\right) \\
& + 4\mathrm{i}\sigma^{-4}F^3F'C^*C\cosh\left(A^*F\gamma\right)\cosh\left(A^*F\widetilde{\eta}\right)\widetilde{\eta} + \text{c.c.}
\end{aligned}
$$
(C 4)

Adding (C 2) and (C 4), and noting that

$$4\mathrm{i}\sigma^{-4}F^3F'C^*C\widetilde{\eta}\left[\cosh\left(AF\gamma\right)\cosh\left(A^*F\widetilde{\eta}\right)+\cosh\left(A^*F\gamma\right)\cosh\left(AF\widetilde{\eta}\right)\right]+\mathrm{c.c.}=0, \quad (\mathrm{C}\,5)$$

we obtain $G(\xi,\widetilde{\eta})$ as in (3.26).

From (3.17),

$$\frac{\partial\psi_{10}}{\partial\widetilde{\eta}}=-J_w^{-1}x_\xi|_w\left(\frac{1}{2}\frac{\partial^2\widehat{\psi}_0}{\partial\widetilde{\eta}^2}+\mathrm{c.c.}\right), \quad \text{at } \widetilde{\eta}=\gamma. \quad (\mathrm{C}\,6)$$

Using (B 10*b*)

$$\left.\frac{\partial^2\widehat{\psi}_0}{\partial\widetilde{\eta}^2}\right|_{\widetilde{\eta}=\gamma}+\mathrm{c.c.}=-2\mathrm{i}\sigma^{-2}F^2C\sinh\left(AF\gamma\right)+\mathrm{c.c.}=4\sigma^{-2}F^2\mathrm{Im}\{C\sinh\left(AF\gamma\right)\}. \quad (\mathrm{C}\,7)$$

Inserting into (C 6), we obtain $B(\xi)$ as in (3.27).

Appendix D. The power input $\dot{W}_f$ for flat channel walls

The case of flat channel walls can be regarded as the limit with $\epsilon_b=0$. Here, the map is the identity, i.e. $\xi=x$, $\eta=y$ (and $\widetilde{\eta}=\widetilde{y}$). Setting $F(\xi)=1$, $\gamma=1$ and $x_w(\xi)=x$ in (3.19) and (3.20), and noting from (3.22) that $C_0=0$, we get the stream function for the case of flat channel walls

$$\widehat{\psi}_0(x,y)=\mathrm{i}\tfrac{1}{2}x\left[\sinh\left(A\widetilde{y}\right)-A\widetilde{y}\cosh A\right]/\left[\sinh A-A\cosh A\right], \quad (\mathrm{D}\,1)$$

where $A=(1-\mathrm{i})/\sigma$, cf. §3.1. By directly solving the linearized vorticity equation in the (x,y) plane, and invoking the boundary-layer approximation, one can obtain the same solution as in (D 1) for small-amplitude oscillations. The velocity amplitudes $\widehat{u}_0=\partial\widehat{\psi}_0/\partial y$ and $\widehat{v}_0=-\partial\widehat{\psi}_0/\partial x$. Thus,

$$\widehat{u}_0=\mathrm{i}\tfrac{1}{2}\beta^{-1}\left(x/A\right)\left[1-\cosh\left(A\widetilde{y}\right)/\cosh A\right], \quad (\mathrm{D}\,2)$$

$$\widehat{v}_0=-\mathrm{i}\tfrac{1}{2}A^{-1}\left[\widetilde{y}-\sinh(A\widetilde{y})/(A\cosh A)\right]. \quad (\mathrm{D}\,3)$$

From the linearized momentum equation in the x direction, the leading order pressure field is obtained:

$$\widehat{p}_0=-\tfrac{1}{2}\beta^{-1}A^{-1}\left[\tfrac{1}{2}x^2-\left(\tfrac{1}{2}\ell\right)^2\right]. \quad (\mathrm{D}\,4)$$

Here we have imposed the condition at the channel ends, $p_0=0$ at $x=\pm\ell/2$, where $\ell=kL$ is the channel length.

The normal stress on the channel wall is zero, as $\partial v/\partial\widetilde{y}=0$ at $\widetilde{y}=1$. Thus, the power delivered to the flat plate is

$$\dot{W}_f=\frac{1}{2\pi}\int_{-\ell/2}^{\ell/2}\int_0^{2\pi}\left(\widehat{p}_0\mathrm{e}^{-\mathrm{i}t}+\mathrm{c.c.}\right)\sin t\,\mathrm{d}t\mathrm{d}x, \quad \text{at } \widetilde{y}=1, \quad (\mathrm{D}\,5)$$

averaged over one time cycle. The integrand is written from (D 4) as

$$\left[\widehat{p}_0\mathrm{e}^{-\mathrm{i}t}+\mathrm{c.c.}\right]_{\widetilde{y}=1}\sin t=\tfrac{1}{8}\beta^{-1}\left[x^2-\left(\tfrac{1}{2}\ell\right)^2\right]\left(-\mathrm{i}/\mathscr{A}+\mathrm{c.c.}\right)+\text{terms of }\mathrm{e}^{\pm2\mathrm{i}t}, \quad (\mathrm{D}\,6)$$

where

$$\mathscr{A} = 1 - \frac{\tan\left[(1-\mathrm{i})\sigma^{-1}\right]}{(1-\mathrm{i})\sigma^{-1}}. \tag{D 7}$$

The terms of $\mathrm{e}^{2\mathrm{i}t}$ and $\mathrm{e}^{-2\mathrm{i}t}$ have zero time average, hence are suppressed. Substituting into (D 5),

$$\dot{W}_f = \frac{1}{8}\beta^{-1}\left(-\mathrm{i}/\mathscr{A} + \mathrm{c.c.}\right) \int_{-\ell/2}^{\ell/2} \left[x^2 - \left(\frac{1}{2}\ell\right)^2\right] \mathrm{d}x = \frac{1}{6}\beta^{-1}\left(\mathrm{i}/\mathscr{A} + \mathrm{c.c.}\right)\left(\frac{1}{2}\ell\right)^3. \tag{D 8}$$

Upon working out the algebra for $\mathrm{i}/\mathscr{A} + \mathrm{c.c.}$, we get

$$\dot{W}_f = \tfrac{1}{3}\beta^{-1}\sigma\left(\mathscr{A}_1/\mathscr{A}_0\right)\left(\tfrac{1}{2}\ell\right)^3, \tag{D 9}$$

where ℓ is the channel length and

$$\mathscr{A}_0 = \left[1 - \frac{\sigma \sinh(1/\sigma)\cosh(1/\sigma)}{\cosh^2(1/\sigma)\cos^2(1/\sigma) + \sinh^2(1/\sigma)\sin^2(1/\sigma)}\right]^2$$

$$+ \left[1 - \frac{\sigma \sin(1/\sigma)\cos(1/\sigma)}{\cosh^2(1/\sigma)\cos^2(1/\sigma) + \sinh^2(1/\sigma)\sin^2(1/\sigma)}\right]^2, \tag{D 10}$$

$$\mathscr{A}_1 = \frac{\sinh(1/\sigma)\cosh(1/\sigma) - \sin(1/\sigma)\cos(1/\sigma)}{\cosh^2(1/\sigma)\cos^2(1/\sigma) + \sinh^2(1/\sigma)\sin^2(1/\sigma)}. \tag{D 11}$$

Note that $\dot{W}_f$ is scaled by $\rho a^2 \omega^3 k^{-2}$ following (2.2), and $\beta = kh$ is the channel width.

REFERENCES

AUERBACH, D., MOEHRING, W. & MOSER, M. 2004 An analytic approach to the Liebau problem of valveless pumping. *Cardiovascular Engng* **4**, 201–207.

DUPEUX, G., LE MERRER, M., LAGUBEAU, G., CLANET, C., HARDT, S. & QUÉRÉ, D. 2011 Viscous mechanism for Leidenfrost propulsion on a ratchet. *Europhys. Lett.* **96**, 58001. doi:10.1209/0295-5075/96/58001.

HARA, T. & MEI, C. C. 1990 Oscillatory flows over periodic ripples. *J. Fluid Mech.* **211**, 183–209.

LONGUET-HIGGINS, M. S. 1953 Mass transport in water waves. *Phil. Trans. R. Soc. Lond.* A **245**, 535–581.

LONGUET-HIGGINS, M. S. 1983 Peristaltic pumping in water waves. *J. Fluid Mech.* **137**, 393–407.

MAHADEVAN, L., DANIEL, S. & CHAUDHURY, M. K. 2004 Biomimetic ratcheting motion of a soft, slender, sessile gel. *Proc. Natl Acad. Sci. USA* **101** (1), 23–26.

MEI, C. C. 1989 *The Applied Dynamics of Ocean Surface Waves*. World Scientific.

MEI, C. C. & YU, J. 1997 The instability of sand ripples under partially standing surface waves. *Phys. Fluids* **9** (6), 1606–1620.

RAYLEIGH, L. 1883 On the circulation of air observed in Kundt's tubes, and on some allied acoustical problems. *Phil. Trans. R. Soc. Lond.* **175**, 1–21.

RINDERKNECHT, D., HICKERSON, A. I. & GHARIB, M. 2005 A valveless micro impedance pump driven by electromagnetic actuation. *J. Micromech. Microengng* **15**, 861–866.

SHAPIRO, A. H., JAFFRIN, M. Y. & WEINBERG, S. L. 1969 Peristaltic pumping with long wavelengths at low Reynolds number. *J. Fluid Mech.* **37**, 799–825.

SPAGNOLIE, S. E. & SHELLEY, M. J. 2009 Shape-changing bodies in fluid: hovering, ratcheting, and bursting. *Phys. Fluids* **21**, 013103.

TAKAGI, D. & BALMFORTH, N. J. 2011 Peristaltic pumping of viscous fluid in an elastic tube. *J. Fluid Mech.* **672**, 196–218.

THIRIA, B. & ZHANG, J. 2010 Ratcheting fluid using geometric anisotropy, *Bulletin of the American Physical Society (APS), Program of the 63rd Annual Meeting of the Division of Fluid Dynamics, Long Beach, California, 2010*, http://meetings.aps.org/link/BAPS.2010.DFD.HC.3.

VAN OEVEREN, R. M. & HOUGHTON, G. 1971 Levitation and counter-gravity motion of spheres by non-uniform hydrodynamic oscillations. *Chem. Engng Sci.* **26**, 1958–1961.

YIN, F. C. P. & FUNG, Y. C. 1971 Comparison of theory and experiment in peristaltic transport. *J. Fluid Mech.* **47**, 93–112.

YU, J. & HOWARD, L. N. 2012 Exact Floquet theory for waves over arbitrary periodic topographies. *J. Fluid Mech.* **712**, 451–470.